AMERICAN SOCIETY FOR MICROBIOLOGY | Journal of Bacteriology

| Bacteriology | Full-Length Text

Calcium signaling controls early stage biofilm formation and dispersal in *Vibrio fischeri*

Jeremy J. Esin,[1] Karen L. Visick,[1] Abby R. Kroken[1]

AUTHOR AFFILIATION See affiliation list on p. 17.

ABSTRACT Bacterial dispersal from a biofilm is presently the least-studied step of the biofilm life cycle. The symbiotic bacterial species *Vibrio fischeri* is a model organism for studying biofilms relevant to a eukaryotic host; however, methodology is lacking to readily study the dispersal of this microbe from biofilms formed in the lab. Here, we adapted a time-lapse assay to visualize biofilm dispersal by *V. fischeri*. We observed biofilm formation and dispersal for multiple *V. fischeri* isolates, which displayed a variety of biofilm architecture phenotypes and dispersal dynamics. We then investigated *V. fischeri* strain ES114 using genetic tools and mutants available for this strain. ES114 exhibited calcium-dependent biofilm formation followed by a rapid (less than 10 min) coordinated dispersal event that occurred approximately 5 h from the experimental start. Biofilm dispersal was largely independent of the dispersal-promoting protease encoded by *lapG*. Although we found no role under our conditions for either biofilm formation or dispersal for several other factors including polysaccharides and autoinducers, we determined that biofilm formation was enhanced, and dispersal was delayed, with increased concentrations of calcium. Furthermore, biofilm formation depended on the calcium-responsive diguanylate cyclase (DGC) CasA, and dispersal could be modulated by overexpressing CasA. Our work has thus developed a new tool for the *V. fischeri* field and uncovered a key role for calcium signaling and c-di-GMP in early biofilm formation and dispersal in *V. fischeri*.

IMPORTANCE Biofilm formation and dispersal are critical steps in both symbiotic and pathogenic colonization. Relative to biofilm formation, the process of dispersal in the model symbiont *Vibrio fischeri*, and other bacteria, is understudied. Here, we adapted an imaging assay to study early biofilm formation and the dispersal process in *V. fischeri*. We demonstrated that our assay can quantify biofilm formation and dispersal over time, can reveal phenotypic differences in diverse natural wild-type isolates, and is sensitive enough to investigate the impact of environmental factors. Our data confirm that calcium is a potent biofilm formation signal and identify the diguanylate cyclase CasA as a key regulator. This work leads the way for more in-depth research about unknown mechanisms of biofilm dispersal.

KEYWORDS video microscopy, *Vibrio fischeri*, biofilms, dispersal, quorum sensing

Biofilm formation is a survival strategy of pathogenic, symbiotic, and environmental bacterial species (1). Biofilms can provide protection from environmental stressors such as antibiotics, host immune-mediated damage, and shear forces (2). Importantly, they can also serve as a reservoir for subsequent infection elsewhere through dispersal, a regulated process that can occur in response to a variety of signals, including starvation and environmental cues (3, 4). Although genetic and environmental factors that promote biofilm formation have been rigorously studied in many microbes, the study of biofilm dispersal can be more challenging to observe and measure. Due to technological

Editor Michael J. Federle, University of Illinois Chicago Pharmaceutical Sciences, Chicago, Illinois, USA

Address correspondence to Karen L. Visick, kvisick@luc.edu, or Abby R. Kroken, akroken@luc.edu.

The authors declare no conflict of interest.

See the funding table on p. 17.

Received 10 March 2025
Accepted 17 April 2025
Published 14 May 2025

advances in microscopy and image analysis and expanded knowledge of the biofilm formation process, the study of biofilm dispersal has become more prevalent in recent years.

The marine bacterium *Vibrio fischeri* has been extensively studied for biofilm formation as it forms and disperses from biofilms to colonize its host, the Hawaiian bobtail squid *Euprymna scolopes* (5). These studies have identified three major pathways critical for the formation of the complex *V. fischeri* biofilm (reviewed in [5]). Two polysaccharides, SYP (symbiosis polysaccharide) and cellulose, and a large adhesive protein, LapV, have been shown to contribute to biofilm formation *in vitro* (6–8). SYP, produced by proteins encoded by the *syp* locus, is best known for its critical role in promoting host-associated biofilm formation and colonization (e.g., [6, 9–11]). SYP fosters cell-cell aggregation and imparts cohesive properties in the laboratory setting (10). However, SYP production is minimal under standard laboratory conditions by the most commonly used wild-type strain, ES114, necessitating the use of genetically manipulated strains for its study. In such strains, it has been shown that biofilm formation can be substantially induced by the introduction of calcium, but not other cations (e.g., [12]).

In contrast to SYP's cell-cell aggregation function, cellulose promotes cell-surface attachment in liquid cultures, for example, to the glass test tube in shaking liquid cultures (9, 10, 12, 13). It also contributes, to a lesser extent, to colony morphology by enhancing wrinkling architecture. Cellulose-dependent phenotypes are also induced by calcium supplementation, particularly at levels of 10 mM (which approximates that present in seawater) and higher (8, 12, 14). This effect occurs in part at the level of transcription of the cellulose genes, *bcs*. Induction of *bcs* transcription by calcium requires the diguanylate cyclase (DGC) CasA and transcription factor VpsR (14).

DGCs function by synthesizing c-di-GMP (Bis-(3′,5′)-cyclic dimeric guanosine monophosphate), a molecule that promotes biofilm formation in many bacteria (5, 15, 16). In turn, c-di-GMP is degraded by phosphodiesterases (PDEs). Many bacterial species encode multiple DGCs and PDEs to fine-tune c-di-GMP levels in response to environmental signals (15). In *V. fischeri*, CasA responds to calcium by synthesizing c-di-GMP via its cytoplasmic GGDEF enzymatic domain (14). Disruption of *casA* prevents both the increase in c-di-GMP levels in response to calcium addition and the associated calcium-dependent phenotypes. These defects are complemented by a wild-type copy of *casA* but not by a mutant derivative with a change in the conserved GGDEF motif (G410A), demonstrating that the calcium-induced changes were caused by CasA-produced c-di-GMP.

Low concentrations of c-di-GMP can promote dispersal from biofilms. For example, in *Pseudomonas fluorescens*, c-di-GMP controls the surface localization of a large adhesive protein, LapA, to mediate the switch between biofilm and dispersal (17–19). When c-di-GMP levels are low, the protease LapG cleaves LapA from the cell surface, promoting dispersal. In contrast, when levels are high, they bind to the inner membrane protein LapD, changing its conformation to permit it to sequester LapG, decreasing dispersal and promoting biofilm formation. In *V. fischeri,* a homologous c-di-GMP-controlled dispersal pathway exists that includes LapD and LapG, along with a non-homologous large adhesive protein, LapV (7). In *V. fischeri*, the deletion of *lapG* increases the proportion of bacteria associated with biofilms in shaking broth cultures, whereas *lapD* mutants exhibit diminished biofilm formation, presumably due to being "locked" into a dispersal state (7). LapV is hypothesized to bind to both SYP and cellulose exopolysaccharides and potentially to surfaces to facilitate both surface attachment and cell-cell interactions in biofilms. Beyond this pathway, however, nothing is known about dispersal in *V. fischeri*.

In this study, we adapted a time-lapse microscopy method developed by Bridges and Bassler (20) to visualize the biofilm formation and dispersal dynamics of *V. fischeri*. We observed different patterns of growth and dispersal for diverse strains of *V. fischeri*. For the best-studied strain, ES114, we observed a coordinated dispersal event that was independent of known autoinducers. Unexpectedly, early biofilm formation did not

require SYP, cellulose, or the LapV surface adhesin. However, calcium was critical for bacterial attachment and accumulation of biofilms. Finally, we identified an important role for the calcium-sensing DGC CasA. Together, these data reveal new biofilm formation and dispersal dynamics as well as describe a key regulatory factor important for these processes in *V. fischeri*.

RESULTS

Squid- and fish-derived isolates of *V. fischeri* exhibit diverse aggregation and dispersal phenotypes

To explore how *V. fischeri* forms and, more importantly, disperses from a biofilm, we adapted the static time-lapse microscopy strategy originally described for *V. cholerae* by Bridges and Bassler (20). Briefly, bacterial samples were diluted, plated into an 8-well borosilicate glass dish, and allowed to attach for 1 h, after which the wells were washed and overlaid with fresh medium prior to imaging. Fields of view containing small groups of attached bacteria, or multiple single cells, were chosen and then imaged every 5 min over 10 h to observe the entire biofilm formation and dispersal lifecycle. We performed these assays using the Tris-buffered tryptone medium tTBS (which supports biofilm formation when calcium is added [21]), in chambers held at 25°C.

ES114 is the most widely studied *V. fischeri* squid isolate, particularly with respect to biofilm formation, but other isolates also obtained from wild-caught squid and fish hosts are studied in laboratory settings (22–27). We evaluated a set of seven isolates for attachment, biofilm size, and dispersal patterns during growth in tTBS containing 10 mM calcium. Strains ES114, MB14A5, MB13B2, KB2B1, ES213, SR5, and MJ11 all attached and formed biofilms, but with some distinct phenotypes (Fig. 1; Movie S1). Strain ES114 attached to the glass bottom, multiplied, formed small biofilms, and then dispersed in a rapid and coordinated manner between 4 and 5 h. ES213 and KB2B1 formed larger aggregates that appeared to disperse later than ES114 (e.g., between 6 and 8 h). MB14A5 and SR5 did not disperse completely in the timeframe of the experiment, whereas MB13B2 and MJ11 formed aggregates with a size similar to ES114 but had delayed dispersal timing. The strains displayed different biofilm formation timing, maximum sizes, and dispersal phenotypes, indicating that different strains of *V. fischeri* recognize and respond in distinct ways to the conditions of our assay. We anticipate that further exploration of these varied isolates will provide additional insights into the mechanisms underlying biofilm formation and coordinated dispersal. Here, we pursued the investigation of dispersal factors in ES114 due to both the larger number of tools available for this strain and the fact that it disperses when the numbers of planktonic individuals are relatively low, making the dispersal event more accessible for imaging and quantification.

Attachment and early aggregation do not depend on SYP, cellulose, or LapV

Considering that biofilm dispersal first requires bacteria to form a biofilm, we tested whether known *V. fischeri* biofilm components were required for attachment, early aggregation, or biofilm formation in our assay. Single mutants with disruptions in genes required for the production of SYP (Δ*sypQ*), cellulose (Δ*bcsA*), and LapV (Δ*lapV*) were evaluated. Previous work from our lab showed that each of these components was at least partially involved in attachment to borosilicate glass during biofilm formation in shaking liquid (7, 12), and therefore, we hypothesized that they would be required here. However, each single mutant exhibited biofilm formation and dispersal phenotypes similar to ES114 (Fig. 2A; Movie S2). These data suggest that the loss of any one of these surface components is not sufficient to disrupt attachment, biofilm formation, or the dispersal process.

To permit subsequent comparisons between replicates, mutant strains, and other experimental conditions, we analyzed each image using a macro designed in the software ImageJ (FIJI) (28). In brief, the macro segments bacterial aggregates from both

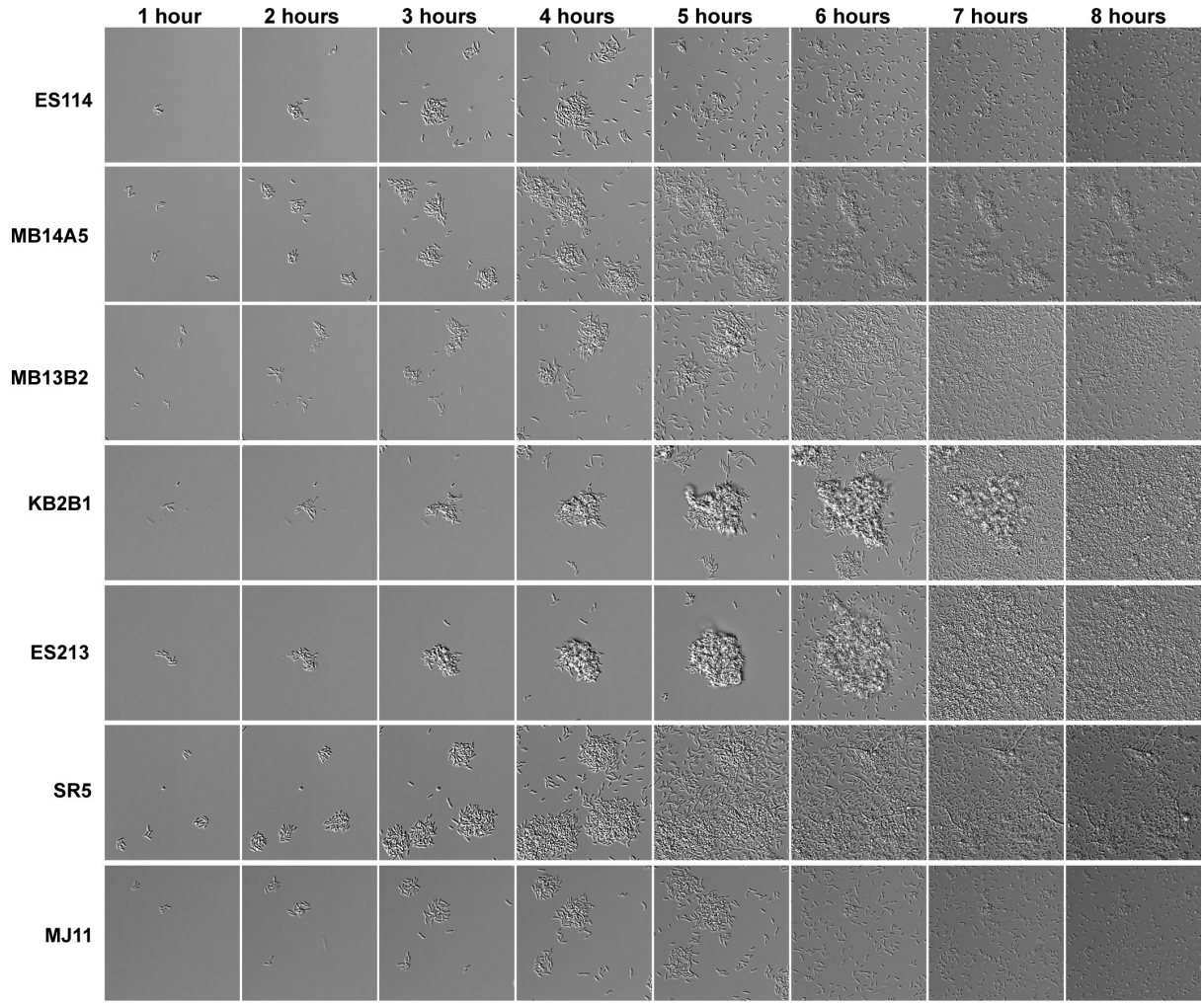

FIG 1 Wild-type squid and fish isolates have diverse biofilm phenotypes. Representative differential interference contrast microscopy (DIC) images from 1–8 h of a 10-h experiment of various wild-type *V. fischeri* isolates. Experiment performed in tTBS containing 10 mM $CaCl_2$ from the point of plate inoculation in room temperature chambers (25°C). Images displayed are 91 µm wide. The images are representative of $n = 3$ biological replicates. The low-contrast vertical banding in images is an artifact from the DS-Qi2 CMOS camera.

background and planktonic bacteria and tracks 2D area over time (see Materials and Methods for further details) (Fig. 2B). Fifteen to 25 individual biofilms were measured from each condition during each experimental replicate, and experiments were repeated two to three times. Since the absolute dispersal time varied between biological replicates (Fig. S1), single representative replicates are shown, and additional replicates are available in supplementary figures. This quantification confirmed that no single surface component deletion was sufficient to alter the pattern of dispersal (Fig. 2C; Movie S2). We thus asked if two or more of these known biofilm factors were necessary by evaluating a triple *bcsA sypQ lapV* mutant that is defective for all three biofilm components. Like the single mutants, the triple mutant also attached, formed a biofilm, and dispersed during time-lapse experiments (Fig. 2A and D; Fig. S2B; Movie S2), although the mutant dispersed from the biofilm 5–20 min earlier than ES114 in each replicate. These data suggest other factor(s) contribute to attachment and steps leading up to early biofilm formation.

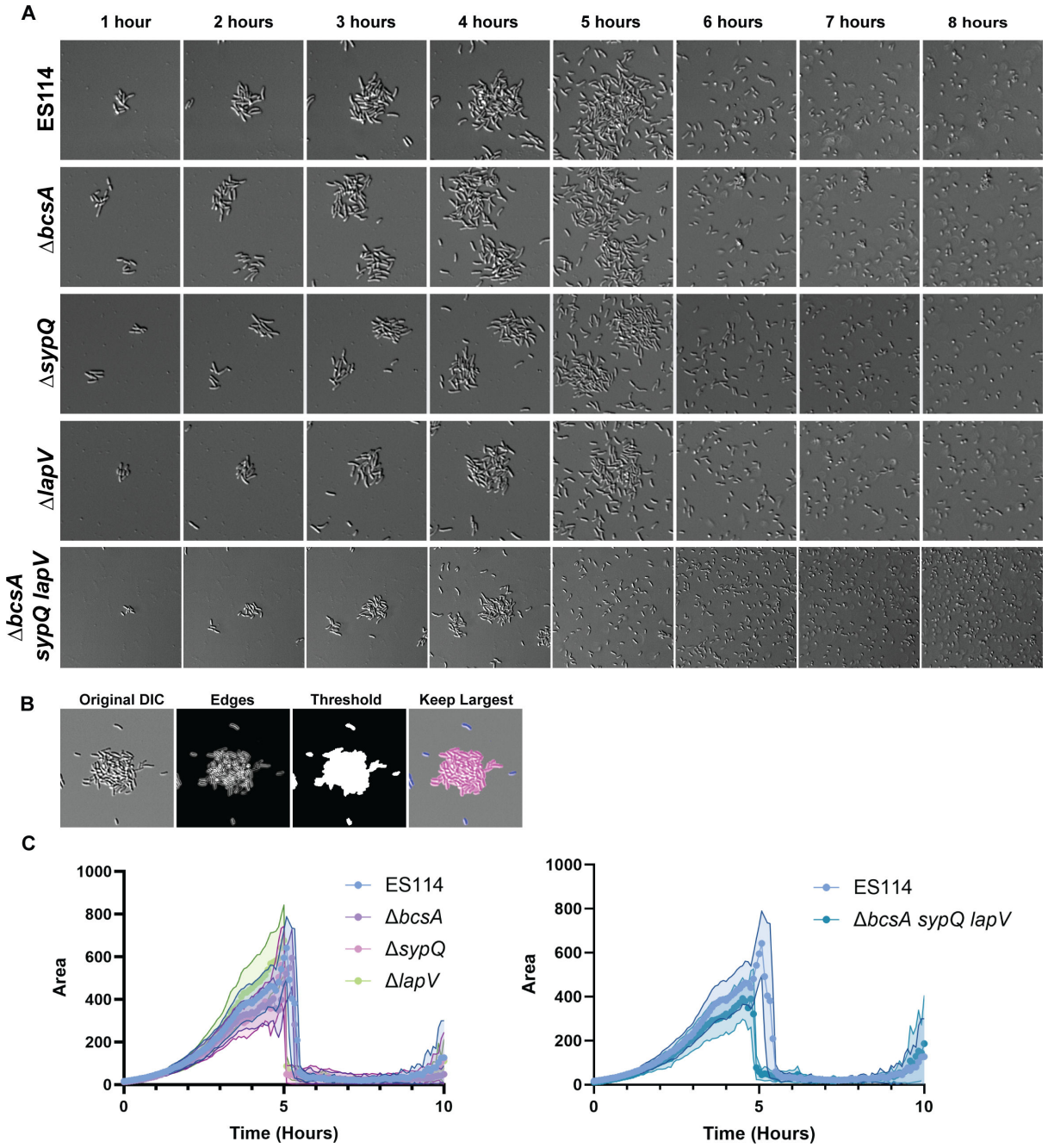

FIG 2 Early aggregation and attachment are independent of SYP, cellulose, and LapV. (A) Representative DIC images from 1–8 h of a 10-h experiment performed as in Fig. 1. (B) Schematic of steps taken in the ImageJ macro used to quantify biofilm area. See text for details. (C) Quantification of biofilm area as measured by time-lapse microscopy from a representative experiment for ES114 and mutants defective for SYP (Δ*sypQ*), cellulose (Δ*bcsA*), or LapV surface adhesin (Δ*lapV-1500*), or a triple mutant deficient for all 3 (Δ*bcsA* Δ*sypQ* Δ*lapV-1500*). Images displayed are 46 µm wide. The images are representative of $n = 3$ biological replicates, and the quantifications include $n = 15–25$ biofilms per condition, ± Standard deviation (SD) (Shaded).

V. fischeri dispersal from early biofilms is largely independent of *lapG*

To evaluate mechanisms of biofilm formation and dispersal under conditions that promote ES114 biofilm formation, we tested a *lapG* protease mutant. LapG-mediated cleavage of the surface adhesin LapV promotes dispersal (7), and thus, we hypothesized that the *lapG* mutant would be incapable of dispersal. Surprisingly, the *lapG* mutant was competent to disperse (Fig. 3A; Movie S3). Quantification revealed that the majority of

the *lapG* mutant cells dispersed in a fashion similar to ES114 (Fig. 3B; Fig. S3). Of note, small areas of biofilm remain attached past the dispersal event, an observation that was consistent across our replicates (Fig. S3). These areas were larger in the *lapG* mutant condition (Fig. 3B, 6–10 h), suggesting that the mutant has a slight defect in biofilm dispersal. The ability of the *lapG* mutant to attach and initiate dispersal suggests that *V. fischeri* uses another pathway(s) to control early biofilm formation and dispersal.

Coordinated dispersal is independent of autoinducer signaling

Given the rapid and coordinated dispersal that we observed (Fig. 2), we postulated that the production and accumulation of autoinducers (29, 30) functions to promote ES114 dispersal. To test this possibility, we evaluated biofilm dispersal by a strain that lacks the three known autoinducers normally produced by *V. fischeri* (i.e., defective for *luxI*, *ainS*, and *luxS*). Contrary to our hypothesis, this triple mutant formed aggregates, achieved a similar overall aggregate area, and dispersed in a coordinated manner comparable with the wild-type parent. While there was some variance between replicates (Fig. 4; Fig. S4; Movie S4), there was no consistent trend toward earlier or later dispersal. These data suggest that autoinducers are not required for early dispersal but leave open the possibility that other secreted molecules could be involved.

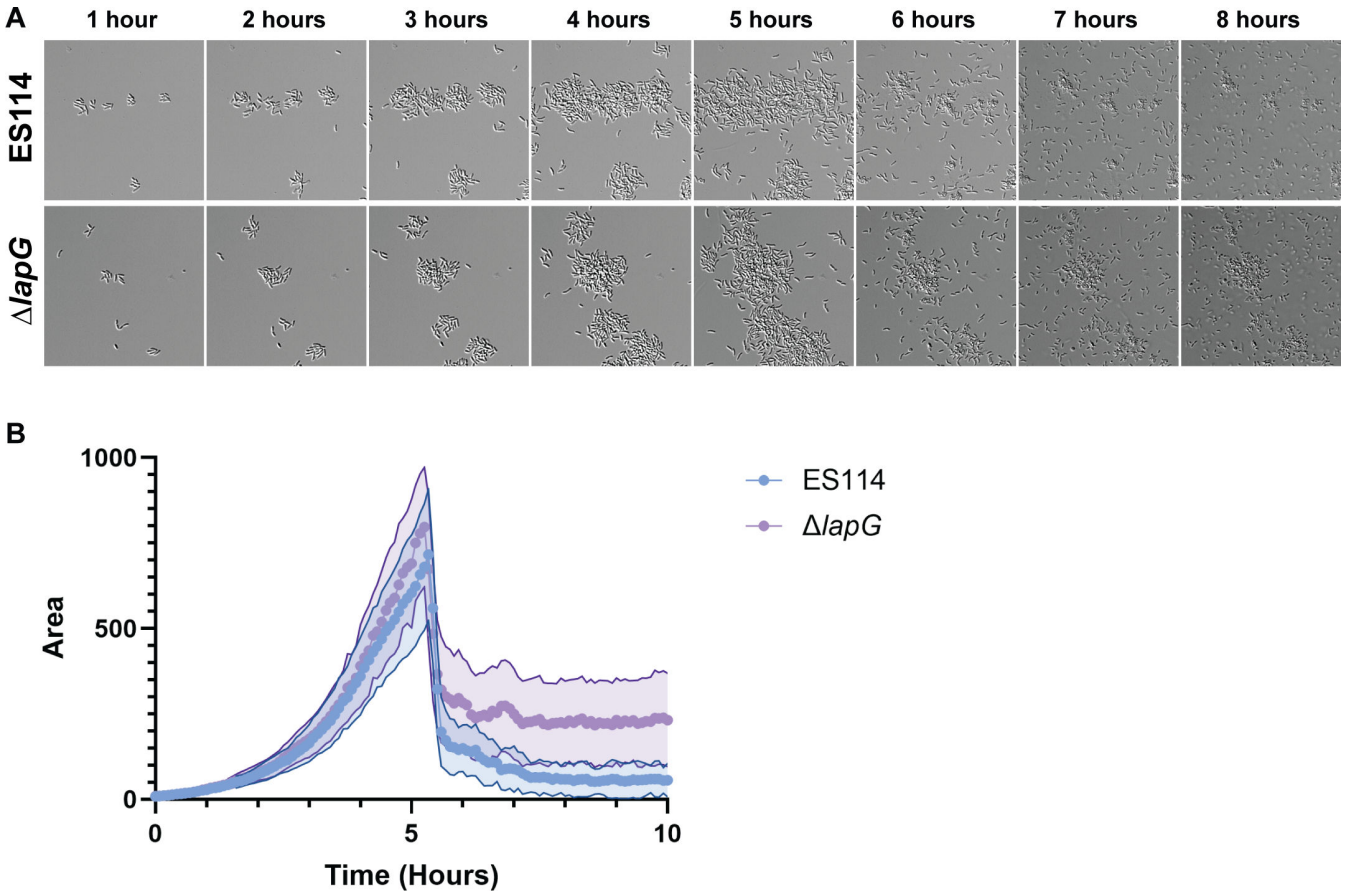

FIG 3 *V. fischeri* dispersal from early biofilms is largely independent of *lap*G. (A) Representative DIC images of 1–8 h of a 10 h experiment, performed as in Fig. 1, comparing ES114 with a strain deficient for LapG (Δ*lapG*). (B) Quantification from a representative experiment via ImageJ macro. Images displayed are 46 µm wide. The images are representative of $n = 3$ biological replicates, and the quantifications include $n = 15–25$ biofilms per condition, ± SD (Shaded).

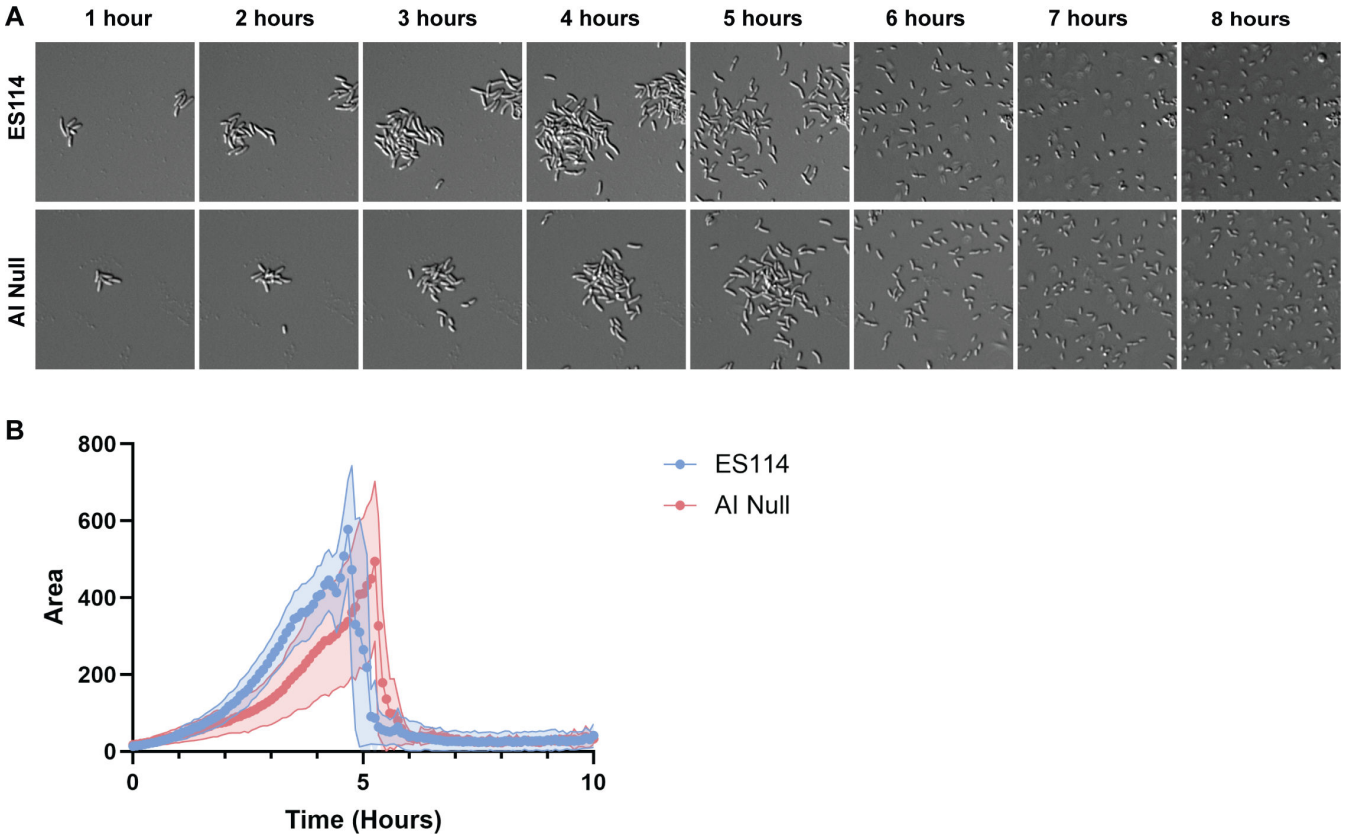

FIG 4 Coordinated dispersal is independent of autoinducer signaling. (A) Representative DIC images of 1–8 h of a 10 h experiment, performed as in Fig. 1, comparing ES114 with a strain deficient for all three autoinducers (*luxI*-frameshift Δ*ainS luxS*). (B) Quantification from a representative experiment via ImageJ macro. Images displayed are 46 µm wide. The images are representative of n = 3 biological replicates, and the quantifications include n = 15–25 biofilms per condition, ± SD (Shaded).

V. fischeri strain ES114 forms and disperses from biofilms when calcium is present

Early biofilm formation and dispersal under our conditions were not impacted by autoinducer signaling, so we investigated environmental signals. Previous research has shown that calcium is a positive signal for biofilm formation in *V. fischeri* (12, 21, 31), but it was unclear if calcium would play a role under the conditions of this new dispersal assay. Thus, we compared the ability of ES114 to form and disperse from biofilms in the presence and absence of 10 mM calcium chloride. When 10 mM calcium chloride was added to tTBS, ES114 readily formed and dispersed from biofilms, as seen previously (e.g., Fig. 1 and 2). In contrast, in non-supplemented tTBS conditions (lacking added calcium), ES114 did not form strong attachments to the glass slide, nor did the strain make multi-cell biofilms (Fig. 5; Movie S5). These data suggest that under our conditions, calcium is required to initiate the biofilm attachment and formation process.

Increasing calcium delays biofilm dispersal

The requirement for calcium addition to induce cell attachment led us to hypothesize that the time of addition and/or concentrations of calcium in our assay could influence biofilm dispersal. First, we asked if the timing of calcium addition could change the outcome of the dispersal assay. The experimental setup includes a 1-h incubation to allow bacterial attachment. We thus compared whether including or excluding calcium during this incubation period changed biofilm formation or dispersal. When calcium was included during the 1-h incubation period, the biofilms formed by ES114 accumulated

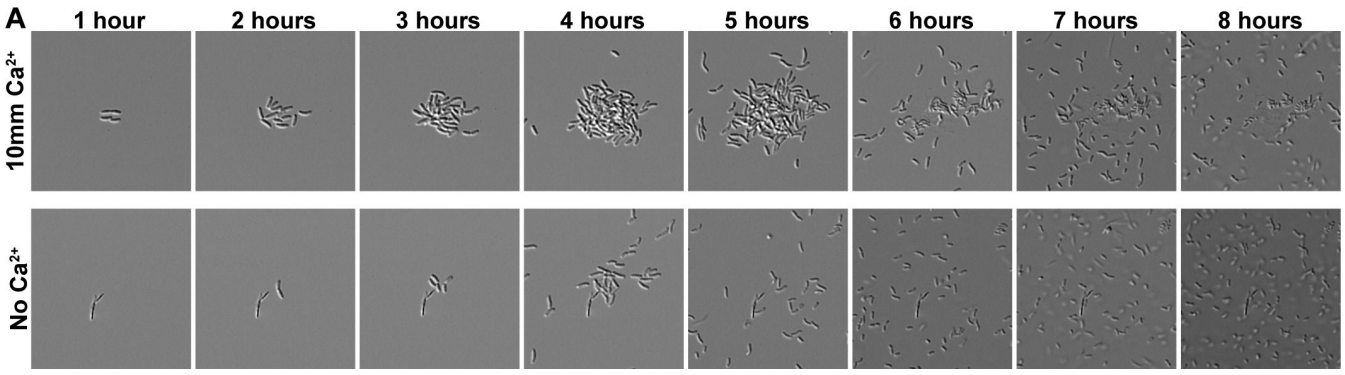

FIG 5 Calcium is required for aggregate formation. Representative DIC images of 1–8 h of a 10 h experiment comparing ES114 in tTBS media with 10 mM added calcium to ES114 in tTBS without added calcium. Other than the inclusion of media that lacks added calcium, the experiment was performed as in Fig. 1. Images displayed are 46 µm wide. *n* = 3 biological replicates.

to occupy larger areas and dispersed later than those that were exposed to calcium after wash steps (Fig. 6A and B; Fig. S5A; Movie S6). These data demonstrate that *V. fischeri* is sensitive to the duration of calcium exposure, which when prolonged results in larger biofilms that disperse later.

Due to the significant effects of a change in the time of calcium addition, we tested if changing the concentration of calcium would alter biofilm formation and dispersal patterns. In our initial experiments, we used calcium at a concentration of 10 mM, which reflects the levels of calcium present in seawater. Previous research in *V. fischeri* demonstrated that calcium concentrations beyond 10 mM can impact other processes, such as motility and c-di-GMP levels (14, 32, 33). We therefore examined the impact of elevated calcium concentrations (20 mM and 40 mM) on biofilm formation and dispersal. Indeed, ES114 produced larger biofilms in response to higher amounts of calcium (Fig. 6C; Movie S6). Strikingly, the timing of dispersal was also delayed when higher amounts of calcium were present, as ES114 reached a maximal biofilm area at later time points (Fig. 6D; Fig. S5B). The appearance of the biofilms in 20 mM and especially in 40 mM calcium was also altered; both had a more rounded and compact structure compared with the 10 mM calcium condition, which consisted of a looser aggregate. The circular structure of ES114 in 40 mM calcium conditions more strongly resembled the biofilms made by ES213 and KB2B1 (compare Fig. 6C with Fig. 1). Overall, these data indicate that calcium exposure, both duration and concentration, can influence biofilm formation, peak biomass, and time of dispersal for *V. fischeri*.

Chelation of free calcium promotes biofilm dispersal

Our data demonstrated that altering calcium concentrations and exposure times influences cellular attachment, biofilm size, and dispersal timing. Therefore, we hypothesized that levels of free calcium could be part of the signal for *V. fischeri* dispersal under our conditions. We thus decreased the levels of free calcium in the middle of biofilm growth by spiking in the calcium chelator EGTA (Ethyleneglycol- *bis*(β-aminoethyl)-N,N,N′,N′-tetraacetic Acid) during a time-lapse experiment of ES114 in tTBS containing 10 mM calcium. Three hours after the experiment was started, EGTA in salt water was added to a final concentration of 10 mM. After the addition of EGTA, bacteria rapidly dispersed from biofilm structures (Fig. 7A; Movie S7). No further structures were formed after EGTA addition to the wells; however, the bacteria continued to grow in the medium, indicating that the EGTA was not lethal to the bacteria. To further assess the effect of the added EGTA on the viability of *V. fischeri*, we measured the growth of *V. fischeri* with shaking over time. The addition of 10 mM EGTA to a culture did not significantly impact the growth of ES114 (Fig. 7B). These data suggest that the addition of the calcium

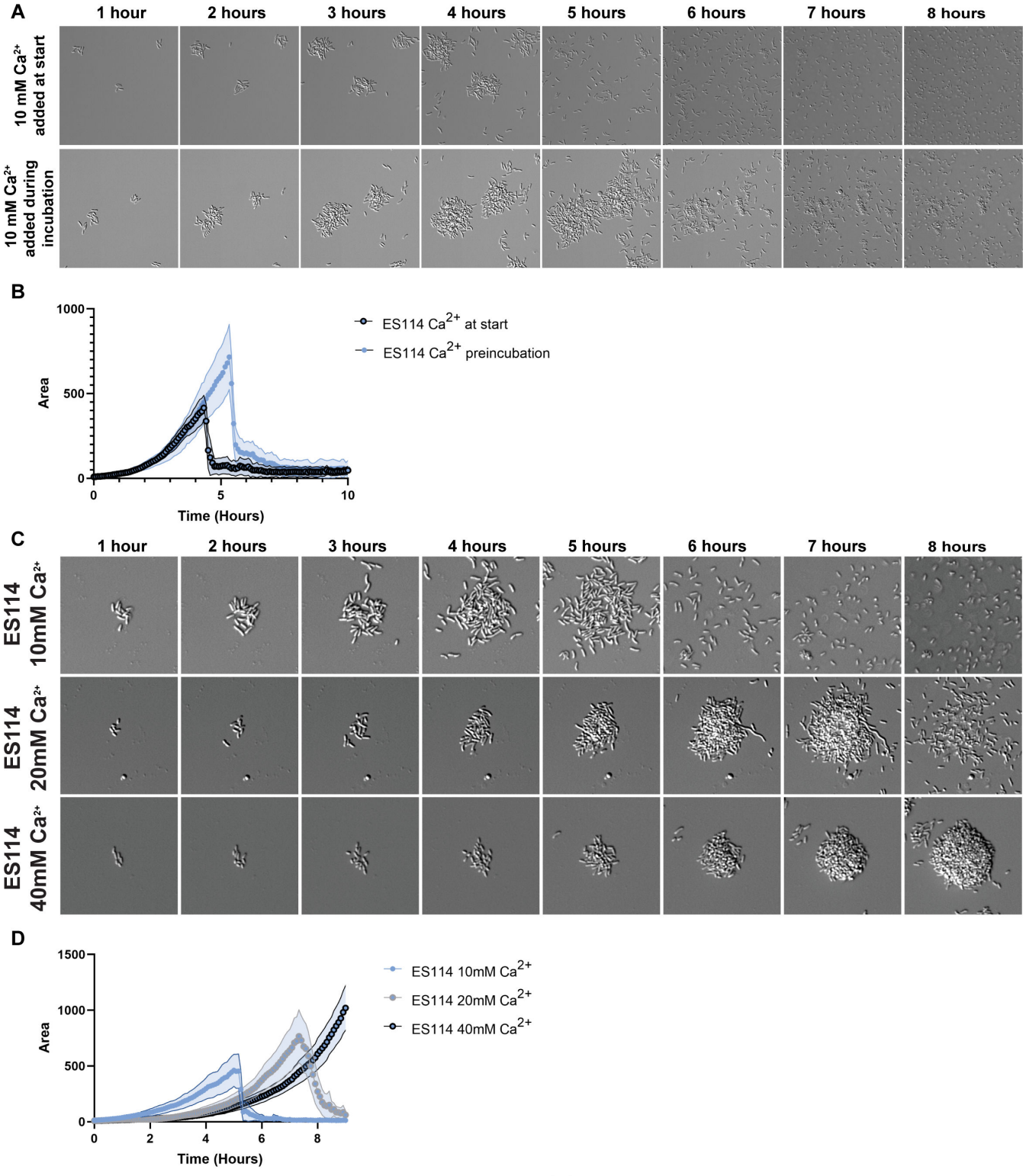

FIG 6 Calcium time of addition and concentration. (A) Representative DIC images of 1–8 h of a 10 h experiment comparing ES114 with 10 mM calcium added just prior to imaging and ES114 that was exposed to 10 mM calcium in the 1 h incubation period. (B) Quantification from a representative panel A experiment via ImageJ macro. (C) Representative DIC images of 1–8 h of a 10 h experiment comparing ES114 in three calcium concentrations (10 mM, 20 mM, and 40 mM). (D) Quantification of a representative experiment for panel C. Images displayed are 46 µm wide. The images are representative of $n = 3$ biological replicates, and the quantifications include $n = 15–25$ biofilms per condition, ± SD (Shaded). The low-contrast vertical banding in panel A is an artifact from the DS-Qi2 CMOS camera.

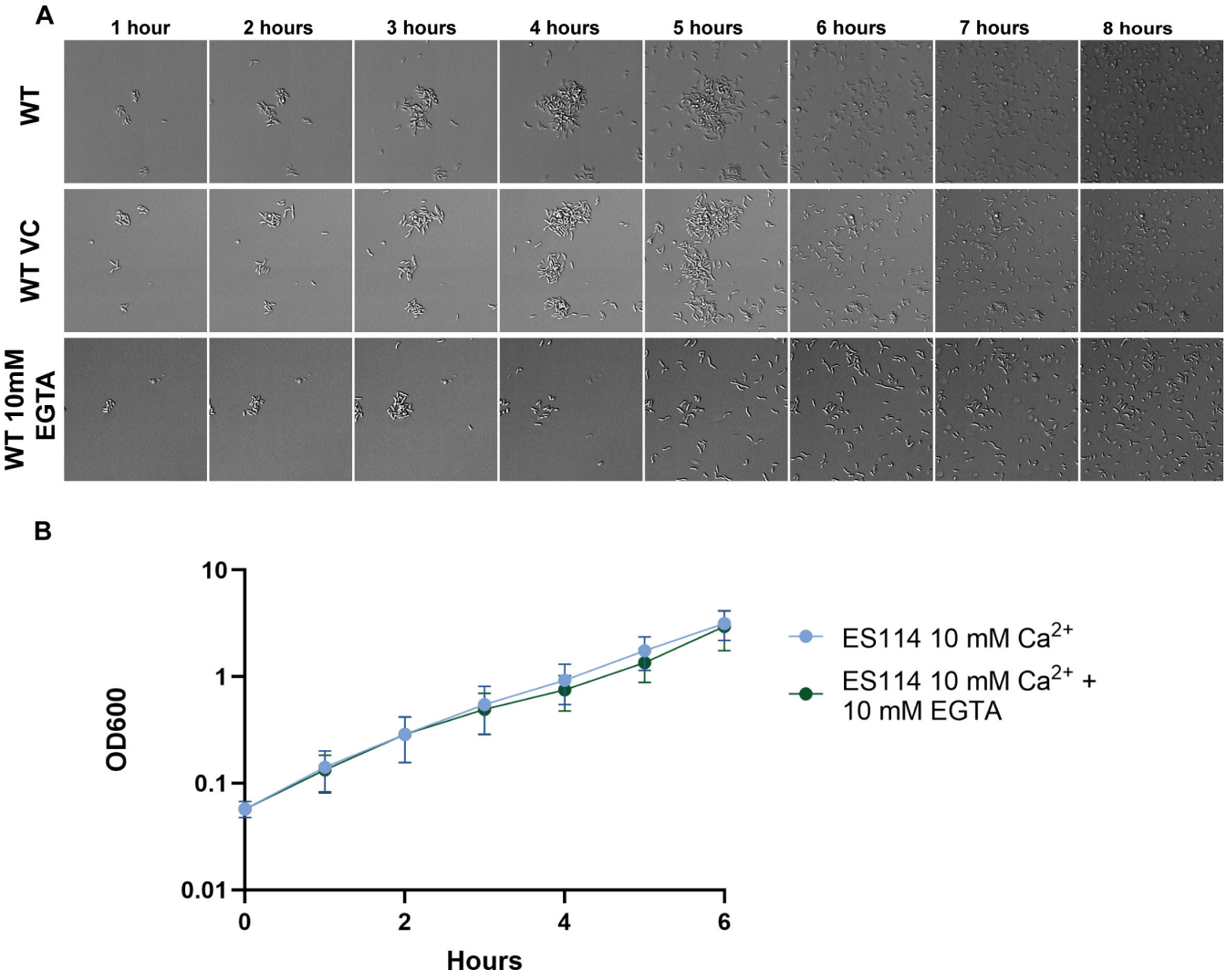

FIG 7 Chelation of free calcium induces dispersal. (A) Representative DIC images of 1–8 h of a 10 h experiment comparing ES114 in tTBS with 10 mM added calcium to ES114 in tTBS with 10 mM added calcium that was either given a vehicle control (VC) of 100 µL saltwater (340 mM NaCl) or 100 µL saltwater containing 10 mM EGTA. The EGTA was added immediately after the 3 h time point was captured. (B) A 6 h growth curve of ES114 in tTBS conditions with 10 mM added calcium and either no addition or 10 mM EGTA added at time zero. A non-linear regression was fitted to each condition using the exponential growth equation. The regression curves were compared to each other and found to not be significant. Images displayed are 46 µm wide. *n* = 3 biological replicates. The low-contrast vertical banding in panel A is an artifact from the DS-Qi2 CMOS camera.

chelator EGTA at 10 mM is not toxic to *V. fischeri* but does induce dispersal in the time-lapse assay.

Calcium sensing is required for biofilm attachment and formation

V. fischeri senses calcium, in part, by the transmembrane calcium-responsive DGC CasA (14). Therefore, we asked if CasA was required to promote biofilm formation in the time-lapse assay. Indeed, a *casA* deletion mutant did not readily attach to the surface or form biofilms in tTBS medium containing 10 mM calcium (Fig. 8A; Movie S8; Fig. S6A). Aggregates were limited to 2–8 individual bacteria at most before they detached from the glass surface. These data suggest that calcium sensing in *V. fischeri* is required for stable attachment.

To verify this result, we tested the phenotype of the Δ*casA* mutant that carried a complementation cassette that was generated previously (14) and consisted of a chromosomal copy of *casA* under the control of a non-native promoter and an idealized

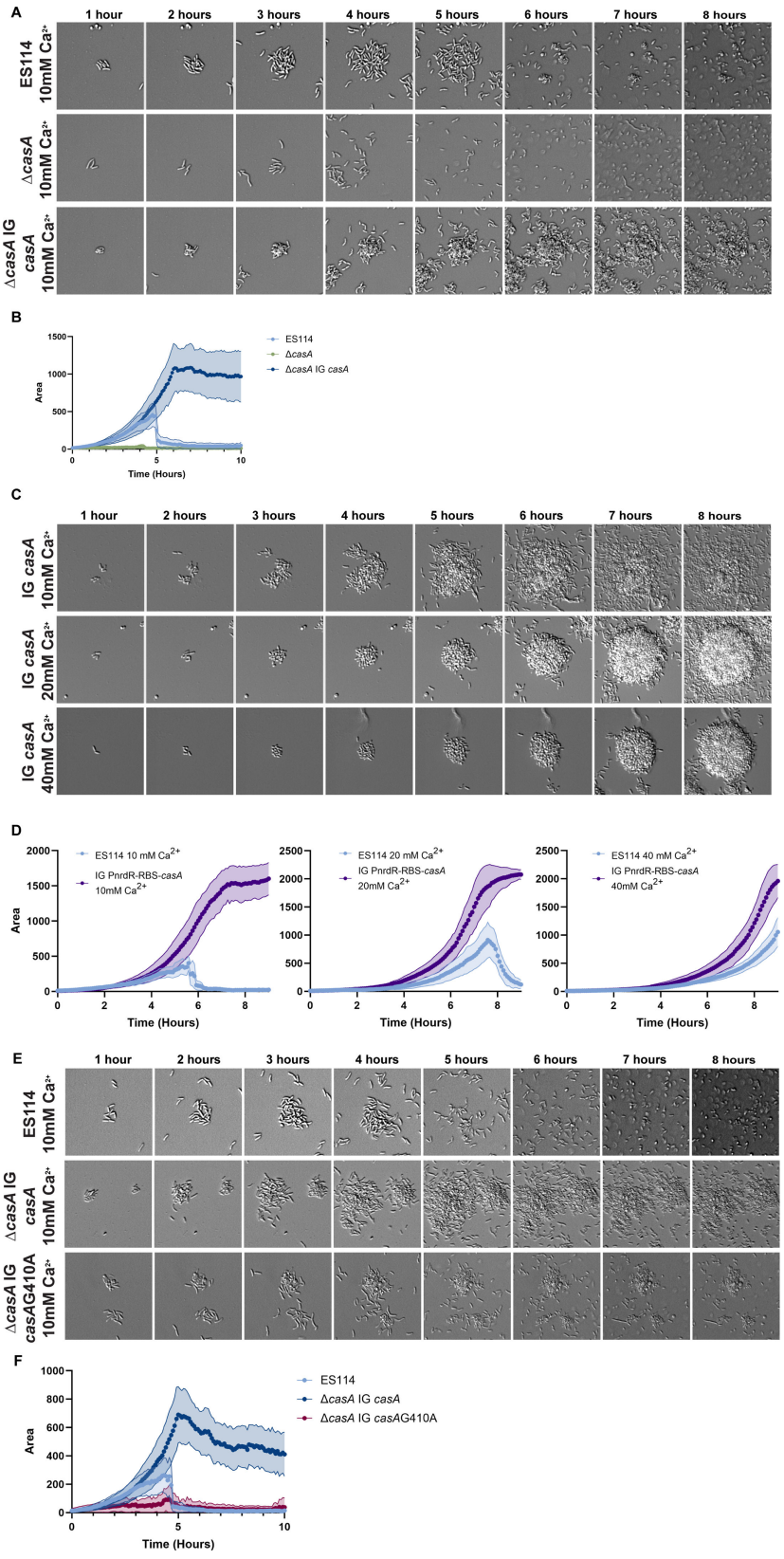

FIG 8 Calcium sensing is required for biofilm attachment and formation. (A) Representative DIC images of 1–8 h of a 10 h experiment comparing ES114 with 10 mM calcium to a strain deleted for *casA* (Δ*casA*) or a strain complemented for *casA* (Δ*casA* IG *casA*). (B) Quantification from a representative panel A

(Continued on next page)

Fig 8 (Continued)

experiment via ImageJ macro. (C) Representative DIC images of 1–8 h of a 10 h experiment comparing a CasA overexpressing strain (IG *casA*) in tTBS media with increasing concentrations of calcium (10 mM, 20 mM, and 40 mM). (D) Quantification from a representative panel C experiment via ImageJ macro. (E) Representative DIC images of 1–8 h of a 10 h experiment comparing ES114 to a strain complemented for casA (Δ*casA* IG *casA*) or a complemented point mutant of *casA* that cannot produce c-di-GMP (Δ*casA* IG *casA*-G410A). (F) Quantification from a representative panel E experiment via ImageJ macro. Images displayed are 46 microns wide. The images are representative of n = 3 biological replicates, and the quantifications include n = 15–25 biofilms per condition, ± SD (Shaded).

ribosome binding site (PnrdR-RBS-*casA*). This strain regained the ability to form a biofilm, suggesting that the loss of CasA was indeed responsible for the inability of the Δ*casA* mutant to form a biofilm. However, the complemented strain unexpectedly failed to disperse. Instead, it formed aggregates that increased in area for about 5 h, which plateaued in size around the same time that ES114 dispersed in a coordinated manner (Fig. 8A; Fig. S6A; Movie S8). Given this result and the construction of the complementation cassette, we conclude that this strain likely overexpresses CasA, causing increased activity and, potentially, increased or prolonged sensitivity to calcium, resulting in a dispersal defect.

This result identified a genetic condition that appeared to impair dispersal. To study this phenomenon further, we generated a *casA* overexpression strain in a wild-type background and included the PnrdR-RBS-*casA* cassette (termed "IG *casA*"). This strain phenocopied the Δ*casA* complemented strain for biofilm formation (Fig. 8A and B; Movie S8). We further tested it by examining its response to increasing amounts of calcium (20 and 40 mM) present in the assay and found that it formed larger aggregates that plateaued at later time points and failed to disperse (Fig. 8C and D; Fig. S6B; Movie S8). This result differs from ES114, which disperses at both the 10 mM and 20 mM conditions (Fig. 8D). These data suggest that either sustained or elevated calcium sensing by CasA blocks biofilm dispersal.

Because CasA is a DGC, we hypothesized that this activity, the production of c-di-GMP, was specifically required. We thus assessed the phenotype of a Δ*casA* mutant that expressed a catalytically inactive derivative of *casA* (G410A) (14) under the control of the same non-native promoter and idealized RBS. This strain failed to form the large biofilms of the Δ*casA* IG PnrdR-RBS-*casA* strain, although it did form small aggregates (Fig. 8E and F; Fig. S7; Movie S8). We conclude that calcium is likely detected by CasA, resulting in increased c-di-GMP levels and therefore increased activation of downstream pathways.

DISCUSSION

In this study, we demonstrated that it is possible to capture the biofilm formation and dispersal process of *V. fischeri* via time-lapse microscopy. We showed that tTBS medium supplemented with 10 mM calcium is a condition sufficient for a productive investigation. We also identified new roles for calcium in controlling both biofilm size and the timing of dispersal. Finally, we found that our assay is broadly applicable to the study of any of a variety of *V. fischeri* strains, as all seven isolates tested formed biofilms under our conditions.

Our time-lapse assay was based on one developed by Bridges and Bassler (20) that we modified for use with *V. fischeri*. In our assay, we employed an area-measurement strategy on individual biofilms captured using differential interference contrast imaging instead of total light attenuation in brightfield. We also adjusted the temperature to 25°C because that temperature promotes *V. fischeri* biofilm formation. In addition, we found that the role of autoinducer between *V. fischeri* and *V. cholerae* differed: in *V. fischeri*, biofilm formation and dispersal patterns did not substantially change when genes for the three autoinducer synthases were deleted, whereas in *V. cholerae,* autoinducers clearly controlled this pathway (20). Of note, the timing of biofilm dispersal by strain ES114 was within about 5–6 h. This is a relatively short dispersal time compared with the 10–12

h timing of *V. cholerae* (34), but it is in line with the known timing of *V. fischeri* biofilm formation and dispersal during squid colonization (35). Our results thus extend the work of Bridges and Bassler (20) by confirming the utility of this imaging-based assay for the discovery of dispersal factors in an additional microbe and by identifying differences both between the two related bacteria and between different *V. fischeri* isolates.

We chose to evaluate biofilm formation and dispersal by representative *V. fischeri* strains that had been differentially assigned into the colonization categories of niche dominant, niche sharing, or ineffectual colonizer (22). We hypothesized, based on previously published data that showed that niche-dominant strains colonize squid hosts faster than the niche-sharing strains (35), that they would form and disperse from biofilms more quickly than the niche-sharing strains under our conditions. However, we could not identify a specific pattern of biofilm formation or dispersal based on niche status. For example, we expected niche-dominant strains MB13B2 and KB2B1 to form a biofilm and disperse quicker than strain ES114 (35), but they did not. Furthermore, MJ11 fails to efficiently colonize *E. scolopes* (11), whereas SR5 can colonize both *Sepiola robusta* and *E. scolopes* (36), but both strains were capable of biofilm formation and dispersal in our time-lapse assay. Of note, both strains lack the sensor kinase RscS, an important regulator of biofilm formation and critical for colonization in many *V. fischeri* strains (11, 37), but this absence did not prevent biofilm formation in this *in vitro* assay. Together, these data indicate that neither colonization differences nor the lack of an important regulator are predictive of dynamics in our *in vitro* assay. This lack of predictive power suggests that our conditions insufficiently match those involved in early colonization steps and that further development of our assay is necessary to observe correlations with colonization. However, there were notable differences (e.g., timing and biofilm sizes) among the strains that are worthy of further investigation.

One surprising result was that neither individual mutants for SYP, cellulose, or Lap nor the triple mutant had biofilm formation or dispersal defects. We expected that deletion of one, and especially all three, would result in lower biofilm formation or attachment. However, our data clearly show these mutants were capable of attachment and biofilm formation. These experiments suggest that there must be one or more other surface components responsible for attachment and initial biofilm formation. Potential components are flagella, LPS molecules, pili, curli, and other polysaccharide(s). In other *Vibrio* species, it has been shown that flagella, although important for motility, also play a role in early biofilm formation by interacting with glass surfaces (38, 39). *V. fischeri* has multiple sheathed (encased in membrane) flagella localized to a single pole of the cell (40). Although some roles have been attributed to the sheathed flagella, many aspects remain unknown, and it is quite possible that a component of the sheath, such as LPS, is required for initial attachment. *V. fischeri* encodes a locus for curli along with nine putative pilus loci, but most remain unstudied (41–43). The potentially redundant nature of the 10 pili loci, including curli, would require the construction of many mutants to determine if pili play a role. Finally, there are other polysaccharides and/or other polysaccharide loci, including *VF_1057-VF0180* (44) and the *vps*-like locus *VF_0352-VF_0344* (45, 46), that could promote binding. The targets described above are only some of the potential candidates, but investigation of these potential factors could lead to a better understanding of the early biofilm formation process.

Calcium was a key factor in successful attachment and aggregate formation in the time-lapse assay. For both the wild-type and *casA* overexpression strains, increased calcium concentrations changed the timing, duration, and size of biofilms. Increased calcium also changed biofilm appearance: when calcium was present at levels of 20 mM or above, the strains produced biofilms with a more uniform round shape that seemed to be taller (a characteristic not captured in our studies). These biofilms more closely resemble the classic mushroom-shaped biofilms reported in other species (47). Our results suggest that because *V. fischeri* is equipped to sense and respond to higher levels of calcium, a niche exists where these bacteria encounter these conditions.

The calcium-sensitive DGC, CasA, was required for stable attachment and biofilm formation. Loss of CasA or disruption of its DGC activity is known to prevent the calcium-induced increase in c-di-GMP levels (14). Given these data and our results with the CasA overproduction strain, we hypothesize that high levels of CasA lead to increased calcium sensitivity and therefore increased c-di-GMP production, which in turn promotes and extends biofilm formation. Correspondingly, the wild-type strain, which both forms and disperses from biofilms, may generate c-di-GMP in response to calcium, then stop making it and/or degrade it. Lower c-di-GMP levels could be achieved in multiple ways, such as through lowered transcription of *casA*, degradation of CasA, or an antagonistic PDE. We hypothesize that whatever the mechanism, it involves specific timing to lower the pool of available c-di-GMP to turn off the pathways activated by CasA and trigger dispersal. Of note, we found that disruption of the enzymatic GGDEF motif did not result in a full null phenotype in our assay; rather than failing to productively attach like its Δ*casA* parent, the CasA-G410A expressing strain attached and formed very small biofilms. These data indicate that CasA-G410A may retain some activity, such as c-di-GMP binding via its RxxD motif (48) or through protein-protein interactions. However, the G410A-overexpression strain failed to form the large biofilms of the CasA-overexpression strain, indicating that diguanylate cyclase activity is critical for that phenotype.

The buildup of c-di-GMP mediated by CasA is thought to activate the transcription factor VpsR which, in turn, activates or represses gene transcription (14). One gene cluster upregulated by VpsR is the *bcs* locus, which is responsible for cellulose production (8, 14). However, based on the lack of a phenotype for the Δ*bcsA* mutant, we conclude that cellulose alone is not responsible for the increased biofilm formation mediated by CasA. These data indicate that the c-di-GMP produced by CasA regulates cell processes via another pathway or that VpsR has another target(s) besides *bcs* that is important for biofilm formation (49).

In summary, we demonstrated that *V. fischeri* biofilm formation and dispersal relies on calcium sensing via CasA and c-di-GMP production in a short-term biofilm formation and dispersal assay. The experimental conditions we tested allowed us to delineate environmental and genetic factors that impact bacterial cell attachment, biofilm accumulation, and dispersal, with the potential to examine these events across multiple strains of *V. fischeri*. Finally, we determined that the early biofilm is independent of already established biofilm components (SYP, Cellulose, and LapV), leaving exciting new directions to explore to understand how *V. fischeri* makes contact with surfaces and undergoes early cell-cell interactions.

MATERIALS AND METHODS

Strains and media

V. fischeri strains, plasmids, and primers used in this study are listed in Tables 1 to 3. ES114 was the parent strain for all genetically manipulated strains. *E. coli* strains were grown in lysogeny broth (LB) (1% tryptone, 0.5% yeast extract, and 1% sodium chloride) (50). For genetic manipulation and routine passaging, *V. fischeri* strains were grown in Luria-Bertani salt (LBS) medium (1% tryptone, 0.5% yeast extract, 2% sodium chloride, and 50 mM Tris, pH 7.5) (51, 52). LB and LBS were solidified with 1.5% agar (final) as appropriate. For imaging experiments, *V. fischeri* strains were grown in Tris-buffered tryptone-based (tTBS) medium (1% tryptone, 2% sodium chloride, and 50 mM Tris, pH 7.5) (21). tTBS medium was supplemented with 10 mM, 20 mM, or 40 mM $CaCl_2$ where noted. For *tfoX*-mediated transformation, Tris-minimal medium (TMM) (300 mM NaCl, 0.1% ammonium chloride, 10 mM *N*-acetylglucosamine, 50 mM $MgSO_4$, 10 mM KCl, 10 mM $CaCl_2$, 0.0058% K_2HPO_4, 10 µM ferrous ammonium sulfate, and 100 mM Tris, pH 7.5) was used (53). For *V. fischeri,* antibiotics were used as follows: erythromycin (Erm), 2.5 µg/mL; trimethoprim (Trim), 10 µg/mL; kanamycin (Kan), 100 µg/mL; and chloramphenicol (Cm), 5 µg/mL. For *E. coli*, antibiotics were used as follows: cm, 12.5 µg/mL; Kan, 50 µg/mL. Thymidine (Thy) was

TABLE 1 Strains used in this study[a,b]

Strain	Genotype	Construction	Reference
CL39	*luxS*::Kan	N/A	(57)
ES114	Sharing isolate from *E. scolopes*	N/A	(58)
ES213	Dominant isolate from *E. scolopes*	N/A	(58)
JE126	Δ*bcsA*::FRT-Trim^R Δ*sypQ*::FRT-Cm^R Δ*lapV*-1500::FRT-Erm^R	TT KV8753 with gKV8613	This study
JE176	Δ*bcsA*::FRT Δ*sypQ*::FRT Δ*lapV*-1500::FRT	Erm^S derivative of JE126 made using pKV496	This study
JE192	*luxI* frameshift Δ*ainS*::FRT-Erm^R	TT VCW2G7 with gKV9367	This study
JE193	*luxI* frameshift Δ*ainS*::FRT-Erm^R *luxS*::Kan^R	TT JE192 with gCL39	This study
JE224	IG::P*nrdR*-RBS-*casA*-HA	TT ES114 with gKV9821	This study
KB2B1	Dominant isolate from *E. scolopes*	N/A	(27)
KV8191	Δ*sypQ*::FRT-Cm^R	N/A	(56)
KV8232	IG::Erm^R-trunc Trim^R	N/A	(56)
KV8613	Δ*lapV-1500*::FRT-Erm^R	N/A	(7)
KV8616	Δ*bcsA*::FRT-Trim^R	N/A	(7)
KV8735	Δ*lapG*::FRT-Erm^R	N/A	(7)
KV8753	Δ*bcsA*::FRT-Trim^R Δ*sypQ*::FRT-Cm^R	N/A	(7)
KV8920	Δ*casA*::FRT-Spec^R	N/A	(14)
KV9367	Δ*ainS*::FRT-Erm^R	N/A	(59)
KV9821	Δ*casA*::FRT-Spec^R IG::P*nrdR*-RBS-*casA*-HA	N/A	(14)
KV9822	Δ*casA*::FRT-Spec^R IG::P*nrdR*-RBS-*casA-G410A*-HA	N/A	(14)
MB13B2	Dominant isolate from *E. scolopes*	N/A	(27)
MB14A5	Sharing isolate from *E. scolopes*	N/A	(27)
MJ11	Isolate from *M. japonica*, colonization-defective in *E. scolopes*	N/A	(42)
SR5	Isolate from *S. robusta*	N/A	(60)
VCW2G7	*luxI* frameshift	N/A	(61)

[a]Abbreviations: FRT, Flp recombinase target; HA, HA epitope-tagged; IG, intragenic region between genes *yeiR* and *glmS*; N/A, not applicable because construction of the indicated strain was constructed reported previously.
[b]Derivation of strains constructed in this study: TT, TfoX-mediated Transformation with a strain containing the *tfoX* gene on a plasmid.

added to a concentration of 0.3 mM for growth of the thymidine auxotroph strain π3813 (54) that carries the conjugal plasmid pEVS104 (55) used to facilitate conjugations and the flippase plasmid pKV496 (56).

Strain construction

Mutations in *V. fischeri* ES114 were generated through TfoX-mediated transformation as described previously (53, 56, 62–64). gDNA was transformed into recipient *V. fischeri* carrying a TfoX-overexpression plasmid pJJC4 (62), and recombinant cells were selected by plating on media containing appropriate antibiotics. Strains were streaked without selection to ensure the TfoX-overexpressing plasmid was lost prior to performing experiments. All genetic manipulations were confirmed by PCR with outside primers using Promega *Taq* polymerase.

TABLE 2 Plasmids used in this study

Name	Description	Reference
pEVS104	Conjugal plasmid	(55)
pJJC4	*tfoX*$^+$ *litR*$^+$ + Cm^R	(62)
pKV496	*flp*$^+$ + Kan^R	(56)
pLosTfox	*tfoX*$^+$ + Cm^R	(63)
pLosTfox-Kan	*tfoX*$^+$ + Kan^R	(64)

TABLE 3 Primers used in this study

Primer number	Sequence[a]
181	aaaaaagaattcAGGATAGATAATAGCGAATAGG
443	CGGTAATACTCCATAAGTTCTTTCAC
1188	GGTAATGCTGGGCGACTAG
1252	ACTTCCACTTGCCGCTATAG
1253	GAATCTTATCGCTTGATGCTTG
1258	GTGTACATAGCTCACCTTCAG
1259	GCAATGGTTGAGATCATGTAAA
1297	ATGGTTGGGCTAAGAGATGGC
1318	ATGTAATCGTACTTTGAGAGCTG
1487	GGTCGTGGGGAGTTTTATCC
2034	CGGTATATAGGAAATTTACAATCTG
2290	AAGAAACCGATACCGTTTACG
2442	TCGCTTGCTTCTACTTCTTTACCTTCTAGTT
2443	CCATTACCATCATCGACAACAATCTCAAAG

[a]Lowercase letters indicate nonbinding or tail sequences.

Time-lapse imaging

Bacteria were prepared from overnight cultures inoculated from single colonies into tTBS and grown overnight at 24°C. Subcultures were started the next day in the same conditions, initially normalized to an optical density of 0.5 at 600 nM (OD_{600}), then grown for seven hours. The cultures were diluted 1:200,000, then seeded into 8-well chambered cover glass (borosilicate) slides (Ibidi) for 1 h in tTBS medium containing or lacking 10 mM $CaCl_2$. Planktonic bacteria were removed by three washes with 500 µL tTBS medium, and a final volume of 500 µL tTBS medium, containing 10 mM $CaCl_2$ or higher levels as noted, was added to each chamber. Time-lapse fields were configured immediately, and imaging began 45 min after the medium change. Images were captured on a Nikon Ti2-E inverted microscope using differential interference contrast. The system was equipped with Nikon perfect focus, an Okolab stage-top incubation chamber held at 25°C, a DS-Qi2 CMOS camera, and a CFI Plan Apochromat Lambda D 40X air NA 0.95 objective. Five fields per well were imaged every 5 min for 10 h. Movies assembled from these images contain all the time points.

Biofilm size measurements

Time-lapse images were computationally analyzed using a custom macro written for the FIJI package of Image J (28). The code for measuring individual biofilms is available in a GitHub repository: [https://github.com/abbykroken/v_fischeri_biofilm/]. In brief, the user is prompted to draw a region of interest (ROI) around a single biofilm; we chose biofilms that did not merge with a neighboring biofilm during the time frame of analysis. The image is registered to account for drift using the Correct 3D Drift plugin (65). Bacteria observed in differential interference contrast are thresholded first by using a Sobel edge detector ("Find Edges"). Within the ROI, isolated planktonic bacteria are removed using a size filter. The largest object (which corresponds to the biofilm during its growth phase) is retained. Its area is calculated for each frame, which is reported as a results table. A color-coded overlay is generated for the user to visually check for accuracy. Loss of the large object corresponds visually to bacterial dispersal.

For each experimental condition, the experiment was performed at least three times on different days. The absolute time of dispersal ranged from 300 min to 360 min for ES114. Thus, the figures show a single experiment representative of three biological replicates, and ES114 was always included as a comparator to observe reproducible trends. Error bars represent variability between 15 and 25 individual biofilms within a biological replicate. We did not further pursue statistical measurements as the observed patterns were striking and generally followed three trends: absence of biofilm, normal

biofilm, and dispersal, or biofilm with delayed/absent dispersal. In Fig. 6C/D&8C/D, we only quantified until hour 9 because at hour 10, there were surrounding planktonic and adhered bacteria that complicated the analyses. Supplemental figures show the variability in each experiment. Movies were assembled using Adobe Premiere.

Time-lapse with EGTA addition

For the EGTA addition experiments, the approach was the same as that described above, except as follows. Three hours after imaging was started, the coverslip was carefully removed, and 100 µL of either vehicle control (VC) of 340 mM salt water or the same saltwater solution containing 60 mM EGTA was gently added to appropriate wells to achieve a final concentration of 10 mM EGTA in a final volume of 600 µL. Our addition of the relatively large volume of 100 µL was designed to facilitate rapid diffusion throughout the sample.

Bacterial growth curves

Single colonies were inoculated into 5 mL of tTBS medium, and the cultures were grown overnight at 24°C with shaking. The next morning, the strains were normalized to an OD_{600} of 0.05 in 30 mL of tTBS in 250 mL baffled flasks, then grown at 24°C with shaking. Calcium was added to a final concentration of 10 mM in each flask, and EGTA was added to 10 mM (final) in indicated flasks prior to inoculation with bacteria. Aliquots of 1 mL were taken hourly for OD_{600} measurements with a spectrophotometer. To maintain accuracy, samples were diluted for measurement when they reached an OD_{600} above 1.0. The graphs were created and statistics were performed with Prism 9 (GraphPad, San Diego, CA, USA). Non-linear regression lines were fit to individual growth curves using exponential growth equations. Curves for each condition were then compared with each other for significant differences.

ACKNOWLEDGMENTS

We thank all the members of the Visick and Stabb labs for technical and experimental discussion, and Kendall Bahl for support.

This work was supported by the National Institutes of Health grants R35 GM130355 (KLV) and R01 EY034239 (ARK).

AUTHOR AFFILIATION

[1]Department of Microbiology and Immunology, Loyola University Chicago, Maywood, Illinois, USA

AUTHOR ORCIDs

Jeremy J. Esin http://orcid.org/0000-0003-1428-2275
Karen L. Visick http://orcid.org/0000-0002-2400-2591
Abby R. Kroken http://orcid.org/0000-0003-1807-1125

FUNDING

Funder	Grant(s)	Author(s)
National Institute of General Medical Sciences	R35GM130355	Karen L. Visick
National Eye Institute	R01EY034239	Abby R. Kroken

AUTHOR CONTRIBUTIONS

Jeremy J. Esin, Conceptualization, Data curation, Formal analysis, Investigation, Methodology, Supervision, Validation, Visualization, Writing – original draft, Writing

– review and editing | Karen L. Visick, Conceptualization, Formal analysis, Funding acquisition, Project administration, Supervision, Writing – original draft, Writing – review and editing | Abby R. Kroken, Conceptualization, Formal analysis, Methodology, Project administration, Software, Supervision, Writing – review and editing

ADDITIONAL FILES

The following material is available online.

Supplemental Material

Supplemental figures (JB00077-25-s0001.pdf). Figures S1 to S7.
Supplemental movie legends (JB00077-25-s0002.pdf). Legends for the Movies S1 to S8.
Movie S1 (JB00077-25-s0003.mp4). Wild type squid and fish isolates have diverse biofilm phenotypes. Representative DIC time-lapse videos of a 10-hour experiment with images taken every 5 minutes. Experiment performed in tTBS containing 10 mM CaCl2 at 25°C. n = 3 biological replicates.
Movie S2 (JB00077-25-s0004.mp4). Early aggregation and attachment are independent of SYP, cellulose, and LapV. Representative DIC time-lapse videos of a 10-hour experiment for ES114 and mutants defective for SYP (ΔsypQ), cellulose (ΔbcsA), or LapV surface adhesin (ΔlapV-1500), or a triple mutant deficient for all three components (ΔbcsA ΔsypQ ΔlapV-1500). n = 3 biological replicates.
Movie S3 (JB00077-25-s0005.mp4). *V. fischeri* dispersal from early biofilms is largely independent of lapG. Representative DIC time-lapse videos of a 10-hour experiment comparing ES114 to a LapG protease deficient strain (ΔlapG). n = 3 biological replicates.
Movie S4 (JB00077-25-s0006.mp4). Coordinated dispersal is independent of auto-inducer signaling. Representative DIC time-lapse videos of a 10-hour experiment comparing ES114 to a strain deficient for all three autoinducers (luxI-frameshift ΔainS luxS). n = 3 biological replicates.
Movie S5 (JB00077-25-s0007.mp4). Calcium is required for aggregate formation. Representative DIC time-lapse video of a 10-hour experiment comparing ES114 in tTBS media with 10 mM added calcium to ES114 in tTBS without added calcium. n = 3 biological replicates.
Movie S6 (JB00077-25-s0008.mp4). Calcium time of addition and concentration. Representative DIC time-lapse videos of a 10-hour experiment comparing ES114 with 10 mM calcium added just prior to imaging, ES114 that was exposed to 10 mM calcium in the 1-hour incubation period, and ES114 in three calcium concentrations (10 mM, 20 mM, 40 mM). n = 3 biological replicates.
Movie S7 (JB00077-25-s0009.mp4). Chelation of free calcium induces dispersal. Representative DIC time-lapse videos of a 10-hour experiment comparing ES114 in tTBS with 10 mM added calcium to ES114 in tTBS with 10 mM added calcium that was either given a vehicle control (VC) of 100 uL saltwater (340 mM NaCl) or 100 uL saltwater containing 10 mM EGTA. n = 3 biological replicates.
Movie S8 (JB00077-25-s0010.mp4). Calcium sensing is required for biofilm attachment and formation. Representative DIC time-lapse videos of a 10-hour experiment comparing ES114 with 10 mM calcium to a strain deleted for casA (ΔcasA), a ΔcasA mutant complemented with either casA (ΔcasA IG casA) or a derivative casA that cannot produce c-di-GMP (ΔcasA IG casA-G410A), and a CasA overexpressing strain (IG casA) in tTBS media with increasing concentrations of calcium (10 mM, 20 mM, 40 mM). n = 3 biological replicates.

REFERENCES

1. Hall-Stoodley L, Costerton JW, Stoodley P. 2004. Bacterial biofilms: from the natural environment to infectious diseases. Nat Rev Microbiol 2:95–108. https://doi.org/10.1038/nrmicro821
2. Flemming HC, Wingender J. 2010. The biofilm matrix. Nat Rev Microbiol 8:623–633. https://doi.org/10.1038/nrmicro2415
3. Tolker-Nielsen T. 2015. Biofilm development. Microbiol Spectr 3:MB–0001. https://doi.org/10.1128/microbiolspec.MB-0001-2014
4. Rumbaugh KP, Sauer K. 2020. Biofilm dispersion. Nat Rev Microbiol 18:571–586. https://doi.org/10.1038/s41579-020-0385-0

5. Fung BL, Esin JJ, Visick KL. 2024. *Vibrio fischeri*: a model for host-associated biofilm formation. J Bacteriol 206:e0037023. https://doi.org/10.1128/jb.00370-23
6. Yip ES, Geszvain K, DeLoney-Marino CR, Visick KL. 2006. The symbiosis regulator RscS controls the *syp* gene locus, biofilm formation and symbiotic aggregation by *Vibrio fischeri*. Mol Microbiol 62:1586–1600. https://doi.org/10.1111/j.1365-2958.2006.05475.x
7. Christensen DG, Marsden AE, Hodge-Hanson K, Essock-Burns T, Visick KL. 2020. LapG mediates biofilm dispersal in *Vibrio fischeri* by controlling maintenance of the VCBS-containing adhesin LapV. Mol Microbiol 114:742–761. https://doi.org/10.1111/mmi.14573
8. Bassis CM, Visick KL. 2010. The cyclic-di-GMP phosphodiesterase BinA negatively regulates cellulose-containing biofilms in *Vibrio fischeri*. J Bacteriol 192:1269–1278. https://doi.org/10.1128/JB.01048-09
9. Yip ES, Grublesky BT, Hussa EA, Visick KL. 2005. A novel, conserved cluster of genes promotes symbiotic colonization and σ^{54}-dependent biofilm formation by *Vibrio fischeri*. Mol Microbiol 57:1485–1498. https://doi.org/10.1111/j.1365-2958.2005.04784.x
10. Shibata S, Yip ES, Quirke KP, Ondrey JM, Visick KL. 2012. Roles of the structural symbiosis polysaccharide (*syp*) genes in host colonization, biofilm formation, and polysaccharide biosynthesis in *Vibrio fischeri*. J Bacteriol 194:6736–6747. https://doi.org/10.1128/JB.00707-12
11. Mandel MJ, Wollenberg MS, Stabb EV, Visick KL, Ruby EG. 2009. A single regulatory gene is sufficient to alter bacterial host range. Nature 458:215–218. https://doi.org/10.1038/nature07660
12. Tischler AH, Lie L, Thompson CM, Visick KL. 2018. Discovery of calcium as a biofilm-promoting signal for *Vibrio fischeri* reveals new phenotypes and underlying regulatory complexity. J Bacteriol 200:e00016-18. https://doi.org/10.1128/JB.00016-18
13. Thompson CM, Tischler AH, Tarnowski DA, Mandel MJ, Visick KL. 2019. Nitric oxide inhibits biofilm formation by *Vibrio fischeri* via the nitric oxide sensor HnoX. Mol Microbiol 111:187–203. https://doi.org/10.1111/mmi.14147
14. Tischler AH, Vanek ME, Peterson N, Visick KL. 2021. Calcium-responsive diguanylate cyclase CasA drives cellulose-dependent biofilm formation and inhibits motility in *Vibrio fischeri*. mBio 12:e0257321. https://doi.org/10.1128/mBio.02573-21
15. Cotter PA, Stibitz S. 2007. c-di-GMP-mediated regulation of virulence and biofilm formation. Curr Opin Microbiol 10:17–23. https://doi.org/10.1016/j.mib.2006.12.006
16. Römling U, Galperin MY, Gomelsky M. 2013. Cyclic di-GMP: the first 25 years of a universal bacterial second messenger. Microbiol Mol Biol Rev 77:1–52. https://doi.org/10.1128/MMBR.00043-12
17. Newell PD, Boyd CD, Sondermann H, O'Toole GA. 2011. A c-di-GMP effector system controls cell adhesion by inside-out signaling and surface protein cleavage. PLoS Biol 9:e1000587. https://doi.org/10.1371/journal.pbio.1000587
18. Navarro MVAS, Newell PD, Krasteva PV, Chatterjee D, Madden DR, O'Toole GA, Sondermann H. 2011. Structural basis for c-di-GMP-mediated inside-out signaling controlling periplasmic proteolysis. PLoS Biol 9:e1000588. https://doi.org/10.1371/journal.pbio.1000588
19. Boyd CD, Chatterjee D, Sondermann H, O'Toole GA. 2012. LapG, required for modulating biofilm formation by *Pseudomonas fluorescens* Pf0-1, is a calcium-dependent protease. J Bacteriol 194:4406–4414. https://doi.org/10.1128/JB.00642-12
20. Bridges AA, Bassler BL. 2019. The intragenus and interspecies quorum-sensing autoinducers exert distinct control over *Vibrio cholerae* biofilm formation and dispersal. PLoS Biol 17:e3000429. https://doi.org/10.1371/journal.pbio.3000429
21. Dial CN, Speare L, Sharpe GC, Gifford SM, Septer AN, Visick KL. 2021. Para-aminobenzoic acid, calcium, and c-di-GMP induce formation of cohesive, Syp-polysaccharide-dependent biofilms in *Vibrio fischeri*. mBio 12:e0203421. https://doi.org/10.1128/mBio.02034-21
22. Bongrand C, Koch EJ, Moriano-Gutierrez S, Cordero OX, McFall-Ngai M, Polz MF, Ruby EG. 2016. A genomic comparison of 13 symbiotic *Vibrio fischeri* isolates from the perspective of their host source and colonization behavior. ISME J 10:2907–2917. https://doi.org/10.1038/ismej.2016.69
23. Koehler S, Gaedeke R, Thompson C, Bongrand C, Visick KL, Ruby E, McFall-Ngai M. 2018. The model squid-vibrio symbiosis provides a window into the impact of strain- and species-level differences during the initial stages of symbiont engagement. Environ Microbiol 21:3269–3283. https://doi.org/10.1111/1462-2920.14392
24. Speare L, Smith S, Salvato F, Kleiner M, Septer AN. 2020. Environmental viscosity modulates interbacterial killing during habitat transition. mBio 11:e03060-19. https://doi.org/10.1128/mBio.03060-19
25. Sun Y, LaSota ED, Cecere AG, LaPenna KB, Larios-Valencia J, Wollenberg MS, Miyashiro T. 2016. Intraspecific competition impacts *Vibrio fischeri* strain diversity during initial colonization of the squid light organ. Appl Environ Microbiol 82:3082–3091. https://doi.org/10.1128/AEM.04143-15
26. Speare L, Cecere AG, Guckes KR, Smith S, Wollenberg MS, Mandel MJ, Miyashiro T, Septer AN. 2018. Bacterial symbionts use a type VI secretion system to eliminate competitors in their natural host. Proc Natl Acad Sci USA 115:E8528–E8537. https://doi.org/10.1073/pnas.1808302115
27. Wollenberg MS, Ruby EG. 2009. Population structure of *Vibrio fischeri* within the light organs of *Euprymna scolopes* squid from two Oahu (Hawaii) populations. Appl Environ Microbiol 75:193–202. https://doi.org/10.1128/AEM.01792-08
28. Schindelin J, Arganda-Carreras I, Frise E, Kaynig V, Longair M, Pietzsch T, Preibisch S, Rueden C, Saalfeld S, Schmid B, Tinevez J-Y, White DJ, Hartenstein V, Eliceiri K, Tomancak P, Cardona A. 2012. Fiji: an open-source platform for biological-image analysis. Nat Methods 9:676–682. https://doi.org/10.1038/nmeth.2019
29. Miyashiro T, Ruby EG. 2012. Shedding light on bioluminescence regulation in *Vibrio fischeri*. Mol Microbiol 84:795–806. https://doi.org/10.1111/j.1365-2958.2012.08065.x
30. Fuqua WC, Winans SC, Greenberg EP. 1994. Quorum sensing in bacteria: the LuxR-LuxI family of cell density-responsive transcriptional regulators. J Bacteriol 176:269–275. https://doi.org/10.1128/jb.176.2.269-275.1994
31. Marsden AE, Grudzinski K, Ondrey JM, DeLoney-Marino CR, Visick KL. 2017. Impact of salt and nutrient content on biofilm formation by *Vibrio fischeri*. PLoS One 12:e0169521. https://doi.org/10.1371/journal.pone.0169521
32. O'Shea TM, Klein AH, Geszvain K, Wolfe AJ, Visick KL. 2006. Diguanylate cyclases control magnesium-dependent motility of *Vibrio fischeri*. J Bacteriol 188:8196–8205. https://doi.org/10.1128/JB.00728-06
33. Shrestha P, Razvi A, Fung BL, Eichinger SJ, Visick KL. 2022. Mutational analysis of *Vibrio fischeri* c-di-GMP-modulating genes reveals complex regulation of motility. J Bacteriol 204:e0010922. https://doi.org/10.1128/jb.00109-22
34. Bridges AA, Fei C, Bassler BL. 2020. Identification of signaling pathways, matrix-digestion enzymes, and motility components controlling *Vibrio cholerae* biofilm dispersal. Proc Natl Acad Sci USA 117:32639–32647. https://doi.org/10.1073/pnas.2021166117
35. Bongrand C, Moriano-Gutierrez S, Arevalo P, McFall-Ngai M, Visick KL, Polz M, Ruby EG. 2020. Using colonization assays and comparative genomics to discover symbiosis behaviors and factors in *Vibrio fischeri*. mBio 11:e03407-19. https://doi.org/10.1128/mBio.03407-19
36. Rotman ER, Bultman KM, Brooks JF 2nd, Gyllborg MC, Burgos HL, Wollenberg MS, Mandel MJ. 2019. Natural strain variation reveals diverse biofilm regulation in squid-colonizing *Vibrio fischeri* J Bacteriol 201:e00033-19. https://doi.org/10.1128/JB.00033-19
37. Visick KL, Skoufos LM. 2001. Two-component sensor required for normal symbiotic colonization of euprymna scolopes by *Vibrio fischeri*. J Bacteriol 183:835–842. https://doi.org/10.1128/JB.183.3.835-842.2001
38. Laventie BJ, Jenal U. 2020. Surface sensing and adaptation in bacteria. Annu Rev Microbiol 74:735–760. https://doi.org/10.1146/annurev-micro-012120-063427
39. Guttenplan SB, Kearns DB. 2013. Regulation of flagellar motility during biofilm formation. FEMS Microbiol Rev 37:849–871. https://doi.org/10.1111/1574-6976.12018
40. Allen RD, Baumann P. 1971. Structure and arrangement of flagella in species of the genus *Beneckea* and *Photobacterium fischeri*. J Bacteriol 107:295–302. https://doi.org/10.1128/jb.107.1.295-302.1971
41. Ruby EG, Urbanowski M, Campbell J, Dunn A, Faini M, Gunsalus R, Lostroh P, Lupp C, McCann J, Millikan D, Schaefer A, Stabb E, Stevens A, Visick K, Whistler C, Greenberg EP. 2005. Complete genome sequence of *Vibrio fischeri*: a symbiotic bacterium with pathogenic congeners. Proc Natl Acad Sci USA 102:3004–3009. https://doi.org/10.1073/pnas.0409900102
42. Mandel MJ, Stabb EV, Ruby EG. 2008. Comparative genomics-based investigation of resequencing targets in *Vibrio fischeri*: focus on point miscalls and artefactual expansions. BMC Genomics 9:138. https://doi.org/10.1186/1471-2164-9-138
43. Barnhart MM, Chapman MR. 2006. Curli biogenesis and function. Annu Rev Microbiol 60:131–147. https://doi.org/10.1146/annurev.micro.60.080805.142106

44. Bennett BD, Essock-Burns T, Ruby EG. 2020. HbtR, a heterofunctional homolog of the virulence regulator TcpP, facilitates the transition between symbiotic and planktonic lifestyles in *Vibrio fischeri*. mBio 11:e01624-20. https://doi.org/10.1128/mBio.01624-20
45. Darnell CL, Hussa EA, Visick KL. 2008. The putative hybrid sensor kinase SypF coordinates biofilm formation in *Vibrio fischeri* by acting upstream of two response regulators, SypG and VpsR. J Bacteriol 190:4941–4950. https://doi.org/10.1128/JB.00197-08
46. Yildiz FH, Visick KL. 2009. *Vibrio* biofilms: so much the same yet so different. Trends Microbiol 17:109–118. https://doi.org/10.1016/j.tim.2008.12.004
47. Sauer K, Stoodley P, Goeres DM, Hall-Stoodley L, Burmølle M, Stewart PS, Bjarnsholt T. 2022. The biofilm life cycle: expanding the conceptual model of biofilm formation. Nat Rev Microbiol 20:608–620. https://doi.org/10.1038/s41579-022-00767-0
48. Christen B, Christen M, Paul R, Schmid F, Folcher M, Jenoe P, Meuwly M, Jenal U. 2006. Allosteric control of cyclic di-GMP signaling. J Biol Chem 281:32015–32024. https://doi.org/10.1074/jbc.M603589200
49. Vander Griend JA, Isenberg RY, Kotla KR, Mandel MJ. 2024. Transcriptional pathways across colony biofilm models in the symbiont *Vibrio fischeri*. mSystems 9:e0081523. https://doi.org/10.1128/msystems.00815-23
50. Davis RW, Botstein D, Roth JR. 1980. A manual for genetic engineering, advanced bacterial genetics. Cold Spring Harbor Laboratory Press.
51. Graf J, Dunlap PV, Ruby EG. 1994. Effect of transposon-induced motility mutations on colonization of the host light organ by *Vibrio fischeri*. J Bacteriol 176:6986–6991. https://doi.org/10.1128/jb.176.22.6986-6991.1994
52. Stabb EV, Reich KA, Ruby EG. 2001. *Vibrio fischeri* genes *hvnA* and *hvnB* encode secreted NAD^+-glycohydrolases. J Bacteriol 183:309–317. https://doi.org/10.1128/JB.183.1.309-317.2001
53. Christensen DG, Tepavčević J, Visick KL. 2020. Genetic manipulation of *Vibrio fischeri*. Curr Protoc Microbiol 59:e115. https://doi.org/10.1002/cpmc.115
54. Le Roux F, Binesse J, Saulnier D, Mazel D. 2007. Construction of a *Vibrio splendidus* mutant lacking the metalloprotease gene *vsm* by use of a novel counterselectable suicide vector. Appl Environ Microbiol 73:777–784. https://doi.org/10.1128/AEM.02147-06
55. Stabb EV, Ruby EG. 2002. RP4-based plasmids for conjugation between *Escherichia coli* and members of the vibrionaceae. Methods Enzymol 358:413–426. https://doi.org/10.1016/s0076-6879(02)58106-4
56. Visick KL, Hodge-Hanson KM, Tischler AH, Bennett AK, Mastrodomenico V. 2018. Tools for rapid genetic engineering of *Vibrio fischeri*. Appl Environ Microbiol 84:e00850-18. https://doi.org/10.1128/AEM.00850-18
57. Lupp C, Ruby EG. 2004. *Vibrio fischeri* LuxS and AinS: comparative study of two signal synthases. J Bacteriol 186:3873–3881. https://doi.org/10.1128/JB.186.12.3873-3881.2004
58. Boettcher KJ, Ruby EG. 1990. Depressed light emission by symbiotic *Vibrio fischeri* of the sepiolid squid *Euprymna scolopes*. J Bacteriol 172:3701–3706. https://doi.org/10.1128/jb.172.7.3701-3706.1990
59. Fung BL, Visick KL. 2025. LitR and its quorum-sensing regulators modulate biofilm formation by *Vibrio fischeri*. J Bacteriol 207:e0047624. https://doi.org/10.1128/jb.00476-24
60. Fidopiastis PM, von Boletzky S, Ruby EG. 1998. A new niche for *Vibrio logei*, the predominant light organ symbiont of squids in the genus *Sepiola*. J Bacteriol 180:59–64. https://doi.org/10.1128/JB.180.1.59-64.1998
61. Lupp C, Urbanowski M, Greenberg EP, Ruby EG. 2003. The *Vibrio fischeri* quorum-sensing systems *ain* and *lux* sequentially induce luminescence gene expression and are important for persistence in the squid host. Mol Microbiol 50:319–331. https://doi.org/10.1046/j.1365-2958.2003.t01-1-03585.x
62. Cohen JJ, Eichinger SJ, Witte DA, Cook CJ, Fidopiastis PM, Tepavčević J, Visick KL. 2021. Control of competence in *Vibrio fischeri*. Appl Environ Microbiol 87:e01962-20. https://doi.org/10.1128/AEM.01962-20
63. Pollack-Berti A, Wollenberg MS, Ruby EG. 2010. Natural transformation of *Vibrio fischeri* requires *tfoX* and *tfoY*. Environ Microbiol 12:2302–2311. https://doi.org/10.1111/j.1462-2920.2010.02250.x
64. Brooks JF II, Gyllborg MC, Cronin DC, Quillin SJ, Mallama CA, Foxall R, Whistler C, Goodman AL, Mandel MJ. 2014. Global discovery of colonization determinants in the squid symbiont *Vibrio fischeri*. Proc Natl Acad Sci USA 111:17284–17289. https://doi.org/10.1073/pnas.1415957111
65. Parslow A, Cardona A, Bryson-Richardson RJ. 2014. Sample drift correction following 4D confocal time-lapse imaging. J Vis Exp 2014:51086. https://doi.org/10.3791/51086